Stabilized Single Current Inverse Source Formulations Based on Steklov-Poincaré Mappings

Stabilized Single Current Inverse Source Formulations Based on Steklov–Poincaré Mappings

Paolo Ricci, *Graduate Student Member, IEEE*, Ermanno Citraro, *Graduate Student Member, IEEE*, Adrien Merlini, *Senior Member, IEEE*, and Francesco P. Andriulli, *Fellow, IEEE*

***Abstract*— The inverse source problem in electromagnetics has proved quite relevant for a large class of applications. When it is coupled with the equivalence theorem, the sources are often evaluated as electric and/or magnetic current distributions on an appropriately chosen equivalent surface. In this context, in antenna diagnostics, in particular, Love solutions, i.e., solutions that radiate zero-fields inside the equivalent surface, are often sought at the cost of an increase of the dimension of the linear system to be solved. In this work, instead, we present a reduced-in-size single current formulation of the inverse source problem that obtains one of the Love currents via a stable discretization of the Steklov-Poincaré boundary operator leveraging dual functions. The new approach is enriched by theoretical treatments and by a further low-frequency stabilization of the Steklov-Poincaré operator based on the quasi-Helmholtz projectors that is the first of its (i.e., low-frequency stabilization) kind in this field. The effectiveness and practical relevance of the new schemes are demonstrated via both theoretical and numerical results.**

***Index Terms*— Boundary-element method, inverse source problem, Love currents, low-frequency breakdown, Steklov-Poincaré operator.**

I. Introduction

THE inverse source problem in electromagnetics, i.e., the recovery of a configuration of sources radiating a given field, has been adopted in a variety of applications ranging from antenna diagnostics to near-to-far-field reconstructions [1], [2], [3]. These sources are often electric and/or magnetic current distributions residing on a conveniently placed equivalent surface that can be tailored to scatter the target field by virtue of the equivalence theorem. These currents have traditionally been found within a boundary element framework on apertures or on arbitrary equivalent surfaces (see [4], [5]). Among inverse source strategies, single current solutions, that reconstruct only one family among electric or magnetic currents, are appealing because of the reduced dimensions of the linear systems to be solved and because of their reduced (numerical) nullspace that is limited to the intrinsic ill-posedness of the problem associated with the nonradiating modes. These strategies, however, have been reported to require more care in the solution process if further physical constraints are not used to ensure a simple relationship between equivalent currents and fields [6], [7]. On the other hand, the double current formulations have non-unique solutions due to the presence of non-radiating currents. Whereas the non-uniqueness can be addressed by selecting a particular solution [8], [9], [10], the numerical ill-conditioning of the matrix, inherited by the ill-posed nature of the inverse problem, remains to be addressed. To this end, truncated singular value decompositions (TSVDs) or Tikhonov regularizations have been used to further regularize the problem [2], [11], [12].

Another feature of interest among inverse source schemes is their capacity to find equivalent Love currents—that are directly related to the tangential fields—which is considered in the literature particularly useful for antenna diagnostics [6], [12]. The Love currents can be obtained by adding further constraints to double current formulations [6], [13], [14] or by filtering any of the solution via Calderón projection [15]. Another interesting approach, leveraging Huygens radiators and valid for plane waves, has been proposed in [16] to reduce the size of the Love-constrained problem to that of a single current formulation, at the price of an approximation.

In this work, we follow a different approach. While still targeting a single current formulation, we leveraged dual discretizations to avoid approximating the relationships linking electric and magnetic currents. The contribution of this article is then twofold: we present a new single current formulation capable of obtaining Love currents by leveraging a stable discretization of the Steklov-Poincaré operator [17] without resorting to any approximations of the electromagnetic relations. This results in a single current formulation that delivers one of the Love currents. A similar equation has been used in a different context in [18] and [19]. Differently from what has been presented in those contributions, here we propose a discretization scheme based on dual elements which achieves optimal conditioning despite a higher cost

Manuscript received 5 December 2022; revised 28 June 2023; accepted 12 July 2023. Date of publication 10 August 2023; date of current version 6 October 2023. This work was supported by the European Union (EU) H2020 Research and Innovation Program through the Project COMPETE under the Marie Skłodowska-Curie Grant 955476; from the European Research Council (ERC) through the European Union's Horizon 2020 Research and Innovation Program (Project 321) under Grant 724846; from the Horizon Europe Research and Innovation Program through the Project CEREBRO under the European Innovation Council (EIC) Pathfinder Grant 101046748; and from the Italian Ministry of University and Research through the Program PRIN2017, EMVISIONING, under Grant 2017HZJXSZ, CUP:E64I190025300, and the Program FARE, CELER, under Grant R187PMFXA4. *(Corresponding author: Francesco P. Andriulli.)*

Paolo Ricci, Ermanno Citraro, and Francesco P. Andriulli are with the Department of Electronics and Telecommunications, Politecnico di Torino, 10129 Turin, Italy (e-mail: francesco.andriulli@polito.it).

Adrien Merlini is with the Microwave Department, École Nationale Supérieure Mines-Télécom Atlantique (IMT Atlantique), 29238 Brest, France.

Color versions of one or more figures in this article are available at https://doi.org/10.1109/TAP.2023.3302748.

Digital Object Identifier 10.1109/TAP.2023.3302748

to generate the matrix entries. Moreover, we present the first frequency stabilization of Steklov-Poincaré operators via quasi-Helmholtz projectors and we leverage this new result to stabilize in frequency the new formulations. What we propose is then, to the best of our knowledge, the first low-frequency regularization of a full-wave inverse source scheme showing a high level of accuracy and numerical stability till arbitrarily low-frequencies.

The article is organized as follows: the main electromagnetic operators are introduced in Section II, the new formulations are presented in Section III, whereas Section IV presents the frequency stabilization of the Steklov-Poincaré operator and its application to the new equations. Finally, Section V illustrates the accuracy and stability of the new formulation through numerical test cases. Section VI concludes the latter. Very preliminary results from this work were presented in the conference contribution [20].

II. Background and Notation

Let Γ be a 2-D smooth manifold in $\mathbb{R}^3$ delimiting the internal and external domains Ω^- and Ω^+. Consider a time-harmonic source in Ω^- generating Maxwellian fields in $\Omega^- \cup \overline{\Omega^+} = \mathbb{R}^3$. In light of the equivalence theorem [21], there exist equivalent current densities $\boldsymbol{M}$ and $\boldsymbol{J}$ on Γ which radiate in Ω^+ the same fields as the original source and radiate in Ω^- possibly different electric and magnetic fields; these currents satisfy

$$\boldsymbol{M} = \left(\boldsymbol{E}^+ - \boldsymbol{E}'^-\right) \times \hat{\boldsymbol{n}}_{\boldsymbol{r}} \tag{1}$$

$$\boldsymbol{J} = \hat{\boldsymbol{n}}_{\boldsymbol{r}} \times \left(\boldsymbol{H}^+ - \boldsymbol{H}'^-\right) \tag{2}$$

where $\hat{\boldsymbol{n}}_{\boldsymbol{r}}$ is the unit normal vector to Γ in $\boldsymbol{r}$ pointing toward Ω^+, $\boldsymbol{E}^+$, $\boldsymbol{H}^+$ are the original electric and magnetic field in Ω^+ and $\boldsymbol{E}'^-$ and $\boldsymbol{H}'^-$ are the new fields in Ω^-. The $e^{-\mathrm{i}\omega t}$ time-harmonic dependence is assumed and suppressed throughout the article. Solving the inverse source problem consists in finding a set of equivalent currents $\boldsymbol{M}$, $\boldsymbol{J}$ given the electric and/or magnetic fields' observations on a 2-D smooth and simply connected manifold $\Gamma_m \subset \Omega^+$. These observations are the output of the actual fields' measurement which includes possible probe compensation. We assume a sampling able to capture the degrees of freedom (defined as in [22]) and thus satisfy the equivalence theorem. The problem can be solved naturally by the boundary element method. In this framework, define the electric field integral operator (EFIO) on Γ

$$\mathcal{T}_{\boldsymbol{r}} \boldsymbol{f} = \mathrm{i}k\, \mathcal{T}_{s,\boldsymbol{r}} \boldsymbol{f} + \mathrm{i}k^{-1}\, \mathcal{T}_{h,\boldsymbol{r}} \boldsymbol{f} \tag{3}$$

with

$$\mathcal{T}_{s,\boldsymbol{r}} \boldsymbol{f} = \hat{\boldsymbol{n}}_{\boldsymbol{r}} \times \int_\Gamma \frac{e^{\mathrm{i}k|\boldsymbol{r}-\boldsymbol{r}'|}}{4\pi|\boldsymbol{r}-\boldsymbol{r}'|} \boldsymbol{f}(\boldsymbol{r}')\, \mathrm{d}\boldsymbol{r}' \tag{4}$$

$$\mathcal{T}_{h,\boldsymbol{r}} \boldsymbol{f} = \hat{\boldsymbol{n}}_{\boldsymbol{r}} \times \nabla \int_\Gamma \frac{e^{\mathrm{i}k|\boldsymbol{r}-\boldsymbol{r}'|}}{4\pi|\boldsymbol{r}-\boldsymbol{r}'|} \nabla_s \cdot \boldsymbol{f}(\boldsymbol{r}')\, \mathrm{d}\boldsymbol{r}' \tag{5}$$

and the magnetic field integral operator (MFIO) [23]

$$\mathcal{K}_{\boldsymbol{r}} \boldsymbol{f} = -\hat{\boldsymbol{n}}_{\boldsymbol{r}} \times p.v. \int_\Gamma \nabla \times \frac{e^{\mathrm{i}k|\boldsymbol{r}-\boldsymbol{r}'|}}{4\pi|\boldsymbol{r}-\boldsymbol{r}'|} \boldsymbol{f}(\boldsymbol{r}')\, \mathrm{d}\boldsymbol{r}' \tag{6}$$

where k is the wavenumber and $\boldsymbol{r}$ lies on any 2-D manifold in $\overline{\Omega^+}$ (possibly Γ or Γ_m), to which the definition of $\hat{\boldsymbol{n}}_{\boldsymbol{r}}$ is extended. In the case $\boldsymbol{r} \in \Gamma$ $\mathcal{T}_{\boldsymbol{r}}$, $\mathcal{K}_{\boldsymbol{r}}$ are denoted by $\mathcal{T}$, $\mathcal{K}$, respectively. When $\boldsymbol{r} \in \Gamma_m$, the radiation operator

$$\mathcal{R} = \begin{bmatrix} -\mathcal{K}_{\boldsymbol{r}} & \mathcal{T}_{\boldsymbol{r}} \\ -\mathcal{T}_{\boldsymbol{r}} & -\mathcal{K}_{\boldsymbol{r}} \end{bmatrix} \tag{7}$$

is a linear map between equivalent sources on Γ and observed tangential fields on Γ_m, meaning that

$$\mathcal{R} \begin{bmatrix} -\boldsymbol{M} \\ \eta \boldsymbol{J} \end{bmatrix} = \begin{bmatrix} \hat{\boldsymbol{n}}_{\boldsymbol{r}} \times \boldsymbol{E}^+ \\ \eta \hat{\boldsymbol{n}}_{\boldsymbol{r}} \times \boldsymbol{H}^+ \end{bmatrix} \tag{8}$$

with $\eta = \sqrt{\mu/\epsilon}$ and ϵ, μ being the permittivity and the permeability of the medium, respectively. The inverse problem aims at finding unknown current distributions that satisfy (8), or part of it. Indeed, by selecting a single block of $\mathcal{R}$—either $\mathcal{K}_{\boldsymbol{r}}$ or $\mathcal{T}_{\boldsymbol{r}}$—and solving for the corresponding reduced right-hand side—$\boldsymbol{E}^+$ or $\boldsymbol{H}^+$—four different single current formulations can be obtained. Alternatively, three double current formulations can be derived by considering the full radiator or one of its rows only. The latter systems of continuous equations admit several solutions because multiple equivalent currents can radiate the same external field in Ω^+ and the physical meaning of the solution depends on the type of implicit or explicit additional constraints used to select a particular solution. The Love currents $\boldsymbol{M}_L$, $\boldsymbol{J}_L$ are one of these particular solutions that are obtained by imposing the fields radiated in Ω^- to be identically $\boldsymbol{0}$ [6]. One way of enforcing this condition is to leverage the well-known Calderón projector [24]

$$\mathcal{P}^- = \begin{bmatrix} \frac{\mathcal{I}}{2} + \mathcal{K} & -\mathcal{T} \\ \mathcal{T} & \frac{\mathcal{I}}{2} + \mathcal{K} \end{bmatrix} \tag{9}$$

where $\mathcal{I}$ is the identity operator, that can be added to the system of equations (8) [13] as

$$\begin{bmatrix} \mathcal{R} \\ \mathcal{P}^- \end{bmatrix} \cdot \begin{bmatrix} -\boldsymbol{M}_L \\ \eta \boldsymbol{J}_L \end{bmatrix} = \left[\hat{\boldsymbol{n}}_{\boldsymbol{r}} \times \boldsymbol{E}^+,\, \hat{\boldsymbol{n}}_{\boldsymbol{r}} \times \eta \boldsymbol{H}^+,\, \boldsymbol{0},\, \boldsymbol{0}\right]^T. \tag{10}$$

III. Conforming Discretization of a Steklov-Poincaré-Based Equation

In this section, we introduce a single source method that enforces the Love condition without increasing the matrix system size with regard to standard single source formulations. Starting from the formulation in (10), consider the Love condition expressed with the inner Calderón projector

$$\mathcal{P}^- \begin{bmatrix} -\boldsymbol{M}_L \\ \eta \boldsymbol{J}_L \end{bmatrix} = \boldsymbol{0}. \tag{11}$$

Clearly, for k different from resonant wavenumbers of Γ [25], (11) defines a relation between the two Love currents

$$\eta \boldsymbol{J}_{\boldsymbol{L}} = -\left(\frac{\mathcal{I}}{2} + \mathcal{K}\right)^{-1} \mathcal{T}(-\boldsymbol{M}_L) \tag{12}$$

where $((\mathcal{I}/2) + \mathcal{K})^{-1}\mathcal{T}$ is the Steklov-Poincaré operator [17]. By replacing (12) in the first row equation of (8), we obtain the equation

$$\left(-\mathcal{K}_{\boldsymbol{r}} - \mathcal{T}_{\boldsymbol{r}} \left(\frac{\mathcal{I}}{2} + \mathcal{K}\right)^{-1} \mathcal{T}\right)(-\boldsymbol{M}_L) = \hat{\boldsymbol{n}}_{\boldsymbol{r}} \times \boldsymbol{E}^+ \tag{13}$$

which is a single source equation that naturally yields the magnetic Love current $\boldsymbol{M}_L$. If instead of this current, the electric Love current $\boldsymbol{J}_L$ is desired as the first outcome of the procedure, a similar strategy can be applied obtaining

$$\left(\mathcal{T}_{\boldsymbol{r}} + \mathcal{K}_{\boldsymbol{r}}\mathcal{T}^{-1}\left(\frac{\mathcal{I}}{2} + \mathcal{K}\right)\right)(\eta \boldsymbol{J}_L) = \hat{\boldsymbol{n}}_{\boldsymbol{r}} \times \boldsymbol{E}^{+}. \tag{14}$$

An alternative approach to study (13) and (14) leverages the equivalence theorem, following a similar procedure to the one presented in chapter 3 of [26]. In this context, (13) and (14) can be interpreted as the equations obtained after accordingly changing the material of the internal domain while imposing the Love condition as described in [27].

To numerically solve (13) and (14), the discretization scheme will require particular attention. Starting with (13), the magnetic current is expanded as $\boldsymbol{M}_L(\boldsymbol{r}) \approx \sum_{i=1}^{N_e} m_i \boldsymbol{f}_i(\boldsymbol{r})$ where $\{\boldsymbol{f}_i\}$ are Rao–Wilton–Glisson (RWG) basis functions (here used without edge normalization) and N_e is the number of mesh edges. The electric operator $\mathcal{T}$ is then tested with rotated RWG functions [28] which yields the matrix $\mathbf{T} = \mathrm{i}k\mathbf{T}_s + \mathrm{i}k^{-1}\mathbf{T}_h$, where $[\mathbf{T}_s]_{ij} = \langle \hat{\boldsymbol{n}}_{\boldsymbol{r}} \times \boldsymbol{f}_i, \mathcal{T}_s \boldsymbol{f}_j\rangle_\Gamma$, $[\mathbf{T}_h]_{ij} = \langle \hat{\boldsymbol{n}}_{\boldsymbol{r}} \times \boldsymbol{f}_i, \mathcal{T}_h \boldsymbol{f}_j\rangle_\Gamma$, and $\langle \boldsymbol{a}, \boldsymbol{b}\rangle_\Gamma = \int_\Gamma \boldsymbol{a}(\boldsymbol{r}) \cdot \boldsymbol{b}(\boldsymbol{r})\, \mathrm{d}\boldsymbol{r}$. As a consequence, the $((\mathcal{I}/2) + \mathcal{K})^{-1}$ term must be tested with rotated-RWGs, and to allow for a non-singular discretization of the identity, the source functions used for its discretization must be dual elements [29]—we will use in the following the Buffa–Christiansen (BC) basis functions, a definition of which can be found in [29] and [30]. We define the Gram matrix $[\mathbb{G}]_{ij} = \langle \hat{\boldsymbol{n}}_{\boldsymbol{r}} \times \boldsymbol{f}_i, \boldsymbol{g}_j\rangle_\Gamma$, where $\{\boldsymbol{g}_j(\boldsymbol{r})\}$ denote the BC functions and propose as matrix discretization for the $\mathcal{K}$ operator $[\mathbb{K}]_{ij} = \langle \hat{\boldsymbol{n}}_{\boldsymbol{r}} \times \boldsymbol{f}_i, \mathcal{K}\boldsymbol{g}_j\rangle_\Gamma$. Finally, as a consequence of this choice, the source functions of $\mathcal{T}_{\boldsymbol{r}}$ must be BC functions, and a possible choice for the testing functions are rotated-BC basis functions living on Γ_m. Thus, we define $\mathbb{T}_m = \mathrm{i}k\mathbb{T}_{s,m} + \mathrm{i}k^{-1}\mathbb{T}_{h,m}$ where $\left[\mathbb{T}_{s,m}\right]_{ij} = \langle \hat{\boldsymbol{n}}_{\boldsymbol{r}} \times \boldsymbol{g}_i, \mathcal{T}_{s,\boldsymbol{r}} \boldsymbol{g}_j\rangle_{\Gamma_m}$ and $\left[\mathbb{T}_{h,m}\right]_{ij} = \langle \hat{\boldsymbol{n}}_{\boldsymbol{r}} \times \boldsymbol{g}_i, \mathcal{T}_{h,\boldsymbol{r}} \boldsymbol{g}_j\rangle_{\Gamma_m}$. From the above choices the discretization of the leftmost $\mathcal{K}_{\boldsymbol{r}}$ is entirely determined as $[\mathbf{K}_m]_{ij} = \langle \hat{\boldsymbol{n}}_{\boldsymbol{r}} \times \boldsymbol{g}_i, \mathcal{K}_{\boldsymbol{r}} \boldsymbol{f}_j\rangle_{\Gamma_m}$. By combining the previous discretization schemes we obtain the discretized equation

$$\left(-\mathbf{K}_m - \mathbb{T}_m(\mathbb{G}/2 + \mathbb{K})^{-1}\mathbf{T}\right)(-\mathbf{m}) = \mathbf{e}_m \tag{15}$$

where $[\mathbf{e}_m]_i = \langle \hat{\boldsymbol{n}}_{\boldsymbol{r}} \times \boldsymbol{g}_i, \hat{\boldsymbol{n}}_{\boldsymbol{r}} \times \boldsymbol{E}^{+}\rangle_{\Gamma_m}$ is the discretization of the observed electric field and $\mathbf{m}$ is the vector of solution coefficients m_i. For (14), a similar reasoning leads to

$$\left(\mathbf{T}_m + \mathbb{K}_m\mathbb{T}^{-1}\left(-\mathbb{G}^{\mathrm{T}}/2 + \mathbf{K}\right)\right)(\eta\mathbf{j}) = \varepsilon_m \tag{16}$$

with $\mathbf{T}_m = \mathrm{i}k\mathbf{T}_{s,m} + \mathrm{i}k^{-1}\mathbf{T}_{h,m}$, $\left[\mathbf{T}_{s,m}\right]_{ij} = \langle \hat{\boldsymbol{n}}_{\boldsymbol{r}} \times \boldsymbol{f}_i, \mathcal{T}_{s,\boldsymbol{r}} \boldsymbol{f}_j\rangle_{\Gamma_m}$, $\left[\mathbf{T}_{h,m}\right]_{ij} = \langle \hat{\boldsymbol{n}}_{\boldsymbol{r}} \times \boldsymbol{f}_i, \mathcal{T}_{h,\boldsymbol{r}} \boldsymbol{f}_j\rangle_{\Gamma_m}$, $[\mathbb{K}_m]_{ij} = \langle \hat{\boldsymbol{n}}_{\boldsymbol{r}} \times \boldsymbol{f}_i, \mathcal{K}_{\boldsymbol{r}} \boldsymbol{g}_j\rangle_{\Gamma_m}$, $\mathbb{T} = \mathrm{i}k\mathbb{T}_s + \mathrm{i}k^{-1}\mathbb{T}_h$, $[\mathbb{T}_s]_{ij} = \langle \hat{\boldsymbol{n}}_{\boldsymbol{r}} \times \boldsymbol{g}_i, \mathcal{T}_s \boldsymbol{g}_j\rangle_\Gamma$, $[\mathbb{T}_h]_{ij} = \langle \hat{\boldsymbol{n}}_{\boldsymbol{r}} \times \boldsymbol{g}_i, \mathcal{T}_h \boldsymbol{g}_j\rangle_\Gamma$, $[\mathbf{K}]_{ij} = \langle \hat{\boldsymbol{n}}_{\boldsymbol{r}} \times \boldsymbol{g}_i, \mathcal{K}_{\boldsymbol{r}} \boldsymbol{f}_j\rangle_\Gamma$, $\left[\varepsilon_{mi}\right] = \langle \hat{\boldsymbol{n}}_{\boldsymbol{r}} \times \boldsymbol{f}_i, \hat{\boldsymbol{n}}_{\boldsymbol{r}} \times \boldsymbol{E}^{+}\rangle_{\Gamma_m}$ and $\mathbf{j}$ is the vector of coefficients j_i of the electric current expansion $\boldsymbol{J}_L(\boldsymbol{r}) \approx \sum_{i=1}^{N_e} j_i \boldsymbol{f}_i(\boldsymbol{r})$.

The reader should note that using RWG or BC as testing functions has an important theoretical value and it follows a consolidated practice in the literature (see [7], [13]). At the same time, however, it does not lead to formulations that can be applied directly to a realistic measurement setting to which, however, it can be extended. In fact, we observe that both the RWG and the BC testing functions can be used to interpolate a point-matching scenario. The point-matching strategy can then be handled similarly to previous works in the literature (as in [2], [6], [7], and references therein). Moreover, it should also be noted that it is not necessary to solve both (15) and (16) to obtain both currents: once one of the two currents has been computed (discretized with RWGs), the discretization of the other as a linear combination of BCs can be obtained after back substitution in (12). In addition, only one current is required to compute the probed field in the outside region by using (13) or (14), respectively, following the discretization strategies delineated above with the sole difference that the leftmost operators must be evaluated in the point of interest, and not tested with primal or dual functions. Finally, it is noted that the introduced single-source formulations need the additional inversion of first and second kind operators in (16) and (15), respectively. Thus, the use of (15) should be preferred as the computational overhead of this formulation would be the inversion of $\mathbb{G}/2 + \mathbb{K}$, which is usually well-conditioned and therefore leads to better performances when using the standard iterative solvers present in the literature.

IV. Quasi-Helmholtz Stabilization

The linear system in (16) inherits the well-known low-frequency breakdown of the EFIO, that causes, among other things, the conditioning of the system to grow unbounded as the frequency decreases [31], [32]; at the same time, the linear system in (15) will behave, frequency-wise, like an MFIO requiring low-frequency stabilization to avoid numerical cancellations due to a different behavior over frequency of the solenoidal and non-solenoidal components of fields and solutions [33]. Note that some of the standard inverse source formulations in the literature may also suffer from similar low-frequency problems and may benefit from a stabilization scheme similar to the one proposed below. In this contribution, however, for the sake of brevity, we will limit the analysis to the low-frequency stabilization of our new formulations only. Define $\mathbf{P}_k = \mathbf{P}^{\Lambda H}k^{-1/2} + \mathrm{i}\mathbf{P}^{\Sigma}k^{1/2}$, $\mathbb{P}_k = \mathbb{P}^{\Sigma H}k^{-1/2} + \mathrm{i}\mathbb{P}^{\Lambda}k^{1/2}$, where $\mathbf{P}^{\Sigma} = \Sigma(\Sigma^T\Sigma)^{+}\Sigma^T$, $\mathbf{P}^{\Lambda H} = \mathbf{I} - \mathbf{P}^{\Sigma}$, $\mathbb{P}^{\Lambda} = \Lambda(\Lambda^T\Lambda)^{+}\Lambda^T$, $\mathbb{P}^{\Sigma H} = \mathbf{I} - \mathbb{P}^{\Lambda}$ are the quasi-Helmholtz projectors defined, respectively, in the RWG space and in the dual BC space, $\mathbf{I}$ is the identity matrix, and where Σ, Λ, are the star-to-RWG and loop-to-RWG transformation matrices, the definitions of which can be found in [32]. We indicate with $(\cdot)^{+}$ the Moore–Penrose (MP) pseudoinverse operator. These projectors allow us to separate the components of the solutions with a different behavior over frequency and to rescale them to avoid numerical cancellations. We propose the following regularization schemes for (15) and (16), respectively:

$$\mathbb{P}_k\left(-\mathbf{K}_m - \mathbb{T}_m(\mathbb{G}/2 + \mathbb{K})^{-1}\mathbf{T}\right)\mathbf{P}_k\mathbf{x} = \mathbb{P}_k\mathbf{e}_m \tag{17}$$

$$\mathbf{P}_k\left(\mathbf{T}_m + \mathbb{K}_m\mathbb{T}^{-1}\left(-\mathbb{G}^T/2 + \mathbf{K}\right)\right)\mathbf{P}_k\mathbf{y} = \mathbf{P}_k\varepsilon_m \tag{18}$$

where $-\mathbf{m} = \mathbf{P}_k\mathbf{x}$ and $\eta\mathbf{j} = \mathbf{P}_k\mathbf{y}$. The frequency stability of the above equations will now be demonstrated in two steps: the stabilization of the Steklov-Poincaré operators used in (15), (16) and the one of equations (15), (16)

themselves. First, we will show that quasi-Helmholtz projectors can successfully regularize the Steklov-Poincaré operators in both discretizations presented here. This is proven in (19) and (20), as shown at the bottom of the page, where we exploited standard cancellation properties of projectors on solenoidal spaces [23] (i.e., $\mathbf{P}^{\Lambda H}\mathbf{T}_h = \mathbf{T}_h\mathbf{P}^{\Lambda H} = \mathbb{P}^{\Sigma H}\mathbb{T}_h = \mathbb{T}_h\mathbb{P}^{\Sigma H} = 0$) from which $\mathbf{T}_h = \mathbf{P}^{\Sigma}\mathbf{T}_h\mathbf{P}^{\Sigma}$ and $\mathbb{T}_h = \mathbb{P}^{\Lambda}\mathbb{T}_h\mathbb{P}^{\Lambda}$. In addition in (20), we used the result $\|\mathbf{P}^{\Sigma}\left(-\mathbb{G}^T/2+\mathbf{K}\right)^{-1}\mathbb{P}^{\Lambda}\| = \mathcal{O}\left(k^2\right)$ which follows from $\|\mathbf{P}^{\Sigma}\left(-\mathbb{G}^T/2+\mathbf{K}\right)\mathbb{P}^{\Lambda}\| = \mathcal{O}\left(k^2\right)$ (proven in [23, Sec. IV-B1]) after following a similar procedure as the one in [23, Appendix B]; in (19) the result $\|\mathbb{P}^{\Lambda}(\mathbb{G}/2+\mathbb{K})^{-1}\mathbf{P}^{\Sigma}\| = \mathcal{O}\left(k^2\right)$ which can be proven in a similar and dual way. This ends the proof of the stabilization of the Steklov–Poincaré operator. As a second step, we demonstrate the frequency regularity of (17) noticing that $\mathbb{P}_k\mathbf{K}_m\mathbf{P}_k$ is frequency stable [33] and that $\mathbb{P}_k\mathbb{T}_m(\mathbb{G}/2+\mathbb{K})^{-1}\mathbf{T}\mathbf{P}_k = (\mathbb{P}_k\mathbb{T}_m\mathbb{P}_k)\left(\mathbb{P}_k^{-1}(\mathbb{G}/2+\mathbb{K})^{-1}\mathbf{T}\mathbf{P}_k\right)$ which, following the above developments and the regularity of $\mathbb{P}_k\mathbb{T}_m\mathbb{P}_k$, is the product of two frequency regular operators and thus is frequency regular. Dually the stability and well-conditioning of (18) is proven with $\mathbf{P}_k\mathbb{K}_m\mathbb{T}^{-1}\left(-\mathbb{G}^T/2+\mathbf{K}\right)\mathbf{P}_k = (\mathbf{P}_k\mathbb{K}_m\mathbb{P}_k)\left(\mathbb{P}_k^{-1}\mathbb{T}^{-1}\left(-\mathbb{G}^T/2+\mathbf{K}\right)\mathbf{P}_k\right)$ and the frequency regularity of $\mathbf{P}_k\mathbb{K}_m\mathbb{P}_k$ (on simply-connected geometries), $\mathbb{P}_k^{-1}\mathbb{T}^{-1}\left(-\mathbb{G}^T/2+\mathbf{K}\right)\mathbf{P}_k$, and $\mathbf{P}_k\mathbf{T}_m\mathbf{P}_k$. We conclude this section by noticing that the proposed strategies hold for plane wave sources, but they can be adapted for different excitations by modifying the coefficients of $\mathbf{P}_k$ and $\mathbb{P}_k$ in an analogous way to what would be needed for the EFIO and the MFIO [34]. The extension to different excitation has been omitted from this article for the sake of clarity and brevity. Finally, we highlight that in the implementation of (17) and (18) we explicitly set to 0 the static component of the terms $\mathbf{P}^{\Sigma}\mathbf{K}_m\mathbb{P}^{\Lambda}$, $\mathbb{P}^{\Lambda}\mathbb{K}_m\mathbf{P}^{\Sigma}$, $\mathbf{P}^{\Sigma}\left(-\mathbb{G}^T/2+\mathbf{K}\right)\mathbb{P}^{\Lambda}$, and $\mathbb{P}^{\Lambda}(\mathbb{G}/2+\mathbb{K})\mathbf{P}^{\Sigma}$.

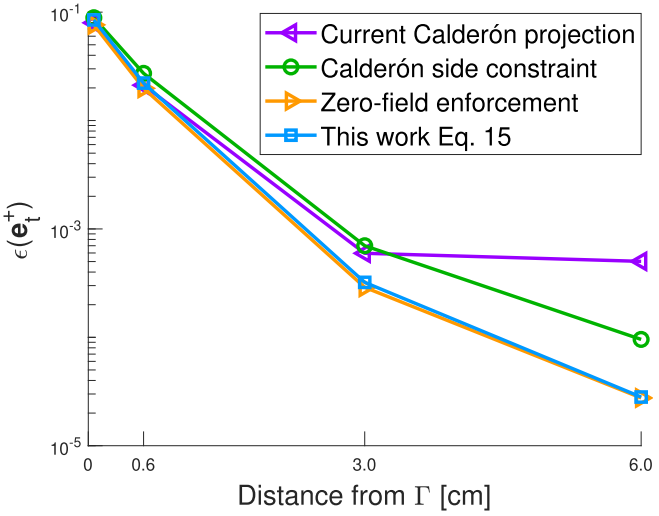

Fig. 1. Field reconstruction error ϵ for the different Love formulations. The fields are obtained from a combination of Hertzian dipoles oscillating at $f = 5$ GHz and noise has been applied to obtain a $SNR = 60$ dB. The field observations are performed on a spherical surface of the same center as Γ and situated 1λ away from Γ. The evaluation of ϵ is then performed on spherical surfaces concentric to Γ with different radii.

V. Numerical Results and Discussion

A series of tests are now presented to demonstrate reconstruction, enforcement of the Love condition, and frequency behavior of the formulation. First the reconstruction capability of the Steklov-Poincaré approach (15) is tested: it maps magnetic currents to electric fields, a most relevant setting for real case scenarios. The electric field of a combination of Hertzian dipoles at frequency $f = 5$ GHz is sampled with ideal probes on a spherical surface Γ_m at $1\lambda = 2\pi/k$ distance from a spherical equivalent surface Γ of radius $a = 6$ cm. The surfaces Γ and Γ_m are discretized with an average mesh edge length of $\lambda/10$ as common in the literature. Similarly

$$\begin{aligned}
\mathbb{P}_k^{-1}\left((\mathbb{G}/2+\mathbb{K})^{-1}\mathbf{T}\right)\mathbf{P}_k &= \left(\sqrt{k}\mathbb{P}^{\Sigma H} + \frac{1}{\mathrm{i}\sqrt{k}}\mathbb{P}^{\Lambda}\right)\left((\mathbb{G}/2+\mathbb{K})^{-1}\left(\mathrm{i}k\mathbf{T}_s + \frac{\mathrm{i}}{k}\mathbf{T}_h\right)\right)\left(\frac{1}{\sqrt{k}}\mathbf{P}^{\Lambda H} + \mathrm{i}\sqrt{k}\mathbf{P}^{\Sigma}\right)\\
&= \mathbb{P}^{\Sigma H}(\mathbb{G}/2+\mathbb{K})^{-1}(\mathrm{i}k\mathbf{T}_s)\mathbf{P}^{\Lambda H} + ik\mathbb{P}^{\Sigma H}(\mathbb{G}/2+\mathbb{K})^{-1}\left(\mathrm{i}k\mathbf{T}_s + \mathrm{i}k^{-1}\mathbf{T}_h\right)\mathbf{P}^{\Sigma}\\
&\quad + (ik)^{-1}\mathbb{P}^{\Lambda}(\mathbb{G}/2+\mathbb{K})^{-1}(\mathrm{i}k\mathbf{T}_s)\mathbf{P}^{\Lambda H} + \mathbb{P}^{\Lambda}(\mathbb{G}/2+\mathbb{K})^{-1}\left(\mathrm{i}k\mathbf{T}_s + \mathrm{i}k^{-1}\mathbf{T}_h\right)\mathbf{P}^{\Sigma}\\
&= -\mathbb{P}^{\Sigma H}(\mathbb{G}/2+\mathbb{K})^{-1}\mathbf{T}_h\mathbf{P}^{\Sigma} + \mathbb{P}^{\Lambda}(\mathbb{G}/2+\mathbb{K})^{-1}\mathbf{T}_s\mathbf{P}^{\Lambda H}\\
&\quad + \mathrm{i}k^{-1}\mathbb{P}^{\Lambda}(\mathbb{G}/2+\mathbb{K})^{-1}\mathbf{P}^{\Sigma}\mathbf{T}_h\mathbf{P}^{\Sigma} + \mathcal{O}(k)\\
&= -\mathbb{P}^{\Sigma H}(\mathbb{G}/2+\mathbb{K})^{-1}\mathbf{T}_h\mathbf{P}^{\Sigma} + \mathbb{P}^{\Lambda}(\mathbb{G}/2+\mathbb{K})^{-1}\mathbf{T}_s\mathbf{P}^{\Lambda H} + \mathcal{O}(k) \qquad (19)\\
\left(\mathbb{P}_k^{-1}\left(\mathbb{T}^{-1}\left(-\mathbb{G}^T/2+\mathbf{K}\right)\right)\mathbf{P}_k\right)^{-1} &= \left(\sqrt{k}\mathbf{P}^{\Lambda H} + \frac{1}{\mathrm{i}\sqrt{k}}\mathbf{P}^{\Sigma}\right)\left(\left(-\mathbb{G}^T/2+\mathbf{K}\right)^{-1}\left(\mathrm{i}k\mathbb{T}_s + \frac{\mathrm{i}}{k}\mathbb{T}_h\right)\right)\left(\frac{1}{\sqrt{k}}\mathbb{P}^{\Sigma H} + \mathrm{i}\sqrt{k}\mathbb{P}^{\Lambda}\right)\\
&= \mathbf{P}^{\Lambda H}\left(-\mathbb{G}^T/2+\mathbf{K}\right)^{-1}(\mathrm{i}k\mathbb{T}_s)\mathbb{P}^{\Sigma H} + ik\mathbf{P}^{\Lambda H}\left(-\mathbb{G}^T/2+\mathbf{K}\right)^{-1}\left(\mathrm{i}k\mathbb{T}_s + \mathrm{i}k^{-1}\mathbb{T}_h\right)\mathbb{P}^{\Lambda}\\
&\quad + (ik)^{-1}\mathbf{P}^{\Sigma}\left(-\mathbb{G}^T/2+\mathbf{K}\right)^{-1}(\mathrm{i}k\mathbb{T}_s)\mathbb{P}^{\Sigma H} + \mathbf{P}^{\Sigma}\left(-\mathbb{G}^T/2+\mathbf{K}\right)^{-1}\left(\mathrm{i}k\mathbb{T}_s + \mathrm{i}k^{-1}\mathbb{T}_h\right)\mathbb{P}^{\Lambda}\\
&= -\mathbf{P}^{\Lambda H}\left(-\mathbb{G}^T/2+\mathbf{K}\right)^{-1}\mathbb{T}_h\mathbb{P}^{\Lambda} + \mathbf{P}^{\Sigma}\left(-\mathbb{G}^T/2+\mathbf{K}\right)^{-1}\mathbb{T}_s\mathbb{P}^{\Sigma H}\\
&\quad + \mathrm{i}k^{-1}\mathbf{P}^{\Sigma}\left(-\mathbb{G}^T/2+\mathbf{K}\right)^{-1}\mathbb{P}^{\Lambda}\mathbb{T}_h\mathbb{P}^{\Lambda} + \mathcal{O}(k)\\
&= -\mathbf{P}^{\Lambda H}\left(-\mathbb{G}^T/2+\mathbf{K}\right)^{-1}\mathbb{T}_h\mathbb{P}^{\Lambda} + \mathbf{P}^{\Sigma}\left(-\mathbb{G}^T/2+\mathbf{K}\right)^{-1}\mathbb{T}_s\mathbb{P}^{\Sigma H} + \mathcal{O}(k) \qquad (20)
\end{aligned}$$

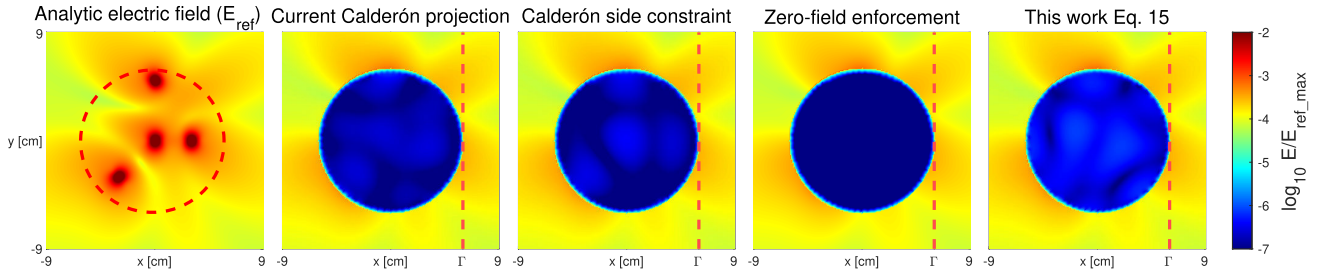

Fig. 2. Modulus of the electric field in a xy planar section of $\mathbb{R}^3$: fields are normalized on the maximum value of the reference field and are obtained from a combination of Hertzian dipoles oscillating at $f = 5$ GHz.

to what is done in [12], noise is added to the sampled fields to obtain a signal-to-noise ratio $SNR = 60$ dB. Our work is then compared to other Love formulations analyzed in [6], [7], and [13] which are three of the several possible approaches that can be found in the literature. The reconstruction capabilities of the formulations are evaluated on several spherical surfaces concentric to Γ, which we define according to the difference between their radius and the one of Γ. On these surfaces, we compute the fields $\mathbf{e}_t$ reconstructed by the different formulations and their error $\epsilon(\mathbf{e}_t)$ with respect to the original noise-less field $\mathbf{e}_{ref}$ radiated by the source. The error is defined as

$$\epsilon(\mathbf{e}_t) := \sqrt{\frac{\sum_{n=1}^{N} |[\mathbf{e}_t]_n - [\mathbf{e}_{ref}]_n|^2}{\sum_{n=1}^{N} |[\mathbf{e}_{ref}]_n|^2}} \tag{21}$$

where N is here used to represent the number of edges of the meshes on which the field is tested. The reconstruction errors obtained in this way in Ω^+ are reported in Fig. 1. We can observe that in this setting all the considered formulations manage to reconstruct the field up to the noise level.

Then, to verify the Love condition, we check whether the internal fields radiated by equivalent currents obtained are zero (within the discretization error) inside the equivalent surface. Results are shown in Fig. 2 where the magnitude of the radiated electric field is displayed on the plane $z = 0$ for the different formulations and qualitatively confirm that all Love formulations find $\sum_{i=1}^{N_e} m_i \boldsymbol{f}_i \approx \boldsymbol{M}_L = -\hat{\boldsymbol{n}}_{\boldsymbol{r}} \times \boldsymbol{E}^+$ on Γ. The better Love condition achieved by the zero-field enforcement method can be attributed to the stronger constraining of the system. Still, a better Love constraining does not imply a better reconstruction of the external fields, as the internal and the external problems are decoupled.

To evaluate the low-frequency behavior of (17), we fix the geometries Γ and Γ_m and we decrease the frequency to $f = 5 \times 10^{-20}$ Hz. The reader should note that, differently from the previous one, the importance of this test is a purely theoretical one. By stably reconstructing a quasi-static setting, in fact, we show that the impact of our new technology encompasses low-frequency scenarios, that, however, will require specific measurement settings [35]. The application of this scheme to these scenarios, however, will be the topic of specific future investigations.

Moreover, as a right-hand side, we use the fields scattered by a perfect electric conductor (PEC) illuminated by a plane wave. The EFIO is used to evaluate the electric currents on a

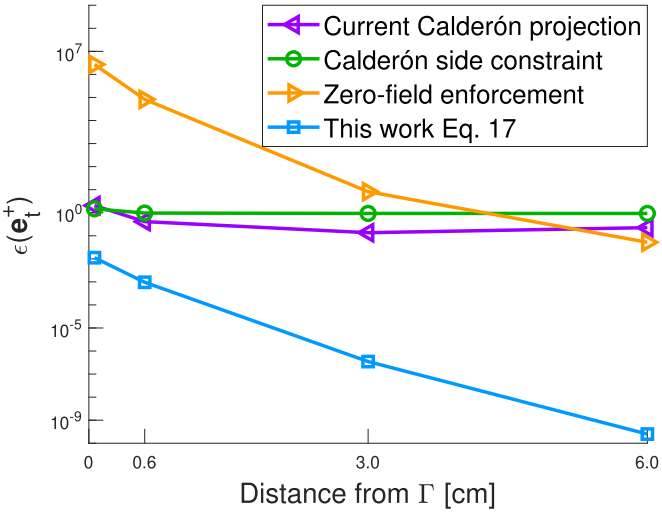

Fig. 3. Field reconstruction error ϵ for the different Love formulations. The equivalent currents and the field samplings are defined on the same meshes used in Fig. 1. The fields are scattered from a 1 cm-radius PEC sphere concentric to Γ illuminated by a plane wave oscillating at $f = 5 \times 10^{-20}$ Hz.

spherical surface Γ_s, concentric to Γ and with a radius of 1 cm, discretized with a triangle mesh composed of 120 edges. The magnetic currents are here not considered as Γ_s is assumed to be a PEC object. Also in this case quasi-Helmoltz projectors are exploited to cure the low-frequency breakdown, resulting in

$$\mathbf{P}_k \mathbf{T} \mathbf{P}_k \mathbf{y} = \mathbf{P}_k \mathbf{e}^i \tag{22}$$

where $\mathbf{e}^i$ is the incident field obtained from a plane wave and tested on Γ_s using RWG basis functions. This equation can be solved by means of standard techniques [23], which include the extraction of the static contribution of the plane wave and the cancellation of $\mathbf{T}_h$ in solenoidal spaces. The solution of (22) can then be used to scatter the fields on Γ_m and on the previously test spheres, whose distance from Γ has not been changed with respect to the previous test. Finally, we employ these fields in an analogous way to what we did in Fig. 1 to study the reconstruction capabilities of the considered formulations also in this setting. As expected, the results in Fig. 3 show that our formulation is the only one still able to correctly reconstruct the field, as the low-frequency breakdown and the numerical cancellations are successfully handled. Similarly to the previous test, by studying the magnitude of the electric field on the plane $z = 0$ we can observe in Fig. 4 that our formulation is still able to enforce the Love condition.

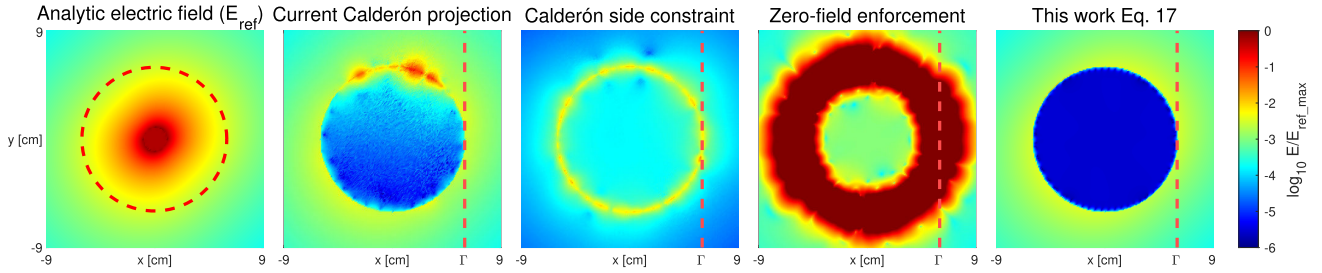

Fig. 4. Modulus of the electric field in a xy planar section of $\mathbb{R}^3$: fields are normalized on the maximum value of the reference field and are obtained from a 1 cm-radius PEC sphere concentric to Γ, excited by a plane wave oscillating at $f = 5 \times 10^{-20}$ Hz.

VI. Conclusion

We have presented a new single current approach that naturally yields Love solutions of the inverse source problem and we have shown that the Love condition is satisfied. Although the presented strategy is currently considered for nonresonant settings, the extension to the resonant setting is possible and will be the focus of further investigations. The technique is enriched by the first frequency stabilization of the Steklov-Poincaré operator via quasi-Helmholtz projectors then used to stabilize the new formulation till arbitrary low frequency. This was then confirmed both by theoretical treatments and by numerical results.

References

[1] Y. A. Lopez, F. Las-Heras Andres, M. R. Pino, and T. K. Sarkar, "An improved super-resolution source reconstruction method," *IEEE Trans. Instrum. Meas.*, vol. 58, no. 11, pp. 3855–3866, Nov. 2009.

[2] E. Jørgensen, P. Meincke, and C. Cappellin, "Advanced processing of measured fields using field reconstruction techniques," in *Proc. 5th Eur. Conf. Antennas Propag. (EUCAP)*, Apr. 2011, pp. 3880–3884.

[3] L. J. Foged, L. Scialacqua, F. Saccardi, J. L. A. Quijano, G. Vecchi, and M. Sabbadini, "Practical application of the equivalent source method as an antenna diagnostics tool [AMTA corner]," *IEEE Antennas Propag. Mag.*, vol. 54, no. 5, pp. 243–249, Oct. 2012.

[4] P. Petre and T. K. Sarkar, "Planar near-field to far-field transformation using an equivalent magnetic current approach," *IEEE Trans. Antennas Propag.*, vol. 40, no. 11, pp. 1348–1356, Nov. 1992.

[5] T. K. Sarkar and A. Taaghol, "Near-field to near/far-field transformation for arbitrary near-field geometry utilizing an equivalent electric current and MoM," *IEEE Trans. Antennas Propag.*, vol. 47, no. 3, pp. 566–573, Mar. 1999.

[6] J. L. A. Quijano and G. Vecchi, "Field and source equivalence in source reconstruction on 3D surfaces," *Prog. Electromagn. Res.*, vol. 103, pp. 67–100, 2010.

[7] J. Kornprobst, R. A. M. Mauermayer, O. Neitz, J. Knapp, and T. F. Eibert, "On the solution of inverse equivalent surface-source problems," *Prog. Electromagn. Res.*, vol. 165, pp. 47–65, 2019.

[8] Y. Alvarez, F. Las-Heras, and M. R. Pino, "Reconstruction of equivalent currents distribution over arbitrary three-dimensional surfaces based on integral equation algorithms," *IEEE Trans. Antennas Propag.*, vol. 55, no. 12, pp. 3460–3468, Dec. 2007.

[9] T. F. Eibert and C. H. Schmidt, "Multilevel fast multipole accelerated inverse equivalent current method employing Rao–Wilton–Glisson discretization of electric and magnetic surface currents," *IEEE Trans. Antennas Propag.*, vol. 57, no. 4, pp. 1178–1185, Apr. 2009.

[10] T. F. Eibert, E. Kaliyaperumal, and C. H. Schmidt, "Inverse equivalent surface current method with hierarchical higher order basis functions, full probe correction and multilevel fast multipole acceleration," *Prog. Electromagn. Res.*, vol. 106, pp. 377–394, 2010.

[11] P. C. Hansen, "The truncated SVD as a method for regularization," *BIT Numer. Math.*, vol. 27, no. 4, pp. 534–553, Dec. 1987.

[12] E. Jørgensen, P. Meincke, C. Cappellin, and M. Sabbadini, "Improved source reconstruction technique for antenna diagnostics," in *Proc. 32nd ESA Antenna Workshop*, 2010, pp. 1–7.

[13] J. Kornprobst, J. Knapp, R. A. M. Mauermayer, O. Neitz, A. Paulus, and T. F. Eibert, "Accuracy and conditioning of surface-source based near-field to far-field transformations," *IEEE Trans. Antennas Propag.*, vol. 69, no. 8, pp. 4894–4908, Aug. 2021.

[14] M. Phaneuf and P. Mojabi, "On the formulation and implementation of the love's condition constraint for the source reconstruction method," *IEEE Trans. Antennas Propag.*, vol. 70, no. 5, pp. 3613–3627, May 2022.

[15] J. Kornprobst, R. A. Mauermayer, E. Kılıç, and T. F. Eibert, "An inverse equivalent surface current solver with zero-field enforcement by left-hand side Calderón projection," in *Proc. 13th Eur. Conf. Antennas Propag. (EuCAP)*, Mar. 2019, pp. 1–3.

[16] T. F. Eibert, D. Vojvodic, and T. B. Hansen, "Fast inverse equivalent source solutions with directive sources," *IEEE Trans. Antennas Propag.*, vol. 64, no. 11, pp. 4713–4724, Nov. 2016.

[17] A. de La Bourdonnaye, "Some formulations coupling finite element and integral equation methods for Helmholtz equation and electromagnetism," *Numerische Math.*, vol. 69, no. 3, pp. 257–268, Jan. 1995.

[18] Z. Guo Qian, W. Cho Chew, and R. Suaya, "Generalized impedance boundary condition for conductor modeling in surface integral equation," *IEEE Trans. Microw. Theory Techn.*, vol. 55, no. 11, pp. 2354–2364, Nov. 2007.

[19] S. Sharma and P. Triverio, "An accelerated surface integral equation method for the electromagnetic modeling of dielectric and lossy objects of arbitrary conductivity," *IEEE Trans. Antennas Propag.*, vol. 69, no. 9, pp. 5822–5836, Sep. 2021.

[20] P. Ricci, A. Merlini, and F. P. Andriulli, "On a frequency-stabilized single current inverse source formulation," in *Proc. IEEE Int. Symp. Antennas Propag. USNC-URSI Radio Sci. Meeting*, Jul. 2022, pp. 1–12.

[21] S. A. Schelkunoff, "Some equivalence theorems of electromagnetics and their application to radiation problems," *Bell Syst. Tech. J.*, vol. 15, no. 1, pp. 92–112, Jan. 1936.

[22] E. Martini and S. Maci, "Generation of complex source point expansions from radiation integrals," *Prog. Electromagn. Res.*, vol. 152, pp. 17–31, 2015.

[23] S. B. Adrian, A. Dély, D. Consoli, A. Merlini, and F. P. Andriulli, "Electromagnetic integral equations: Insights in conditioning and preconditioning," *IEEE Open J. Antennas Propag.*, vol. 2, pp. 1143–1174, 2021.

[24] G. C. Hsiao and R. E. Kleinman, "Mathematical foundations for error estimation in numerical solutions of integral equations in electromagnetics," *IEEE Trans. Antennas Propag.*, vol. 45, no. 3, pp. 316–328, Mar. 1997.

[25] M. Gossye, M. Huynen, D. Van de Ginste, D. De Zutter, and H. Rogier, "A Calderón preconditioner for high dielectric contrast media," *IEEE Trans. Antennas Propag.*, vol. 66, no. 2, pp. 808–818, Feb. 2018.

[26] J.-M. Jin, *Theory and Computation of Electromagnetic Fields*, 2nd ed. Piscataway, NJ, USA: IEEE Press, 2015.

[27] R. F. Harrington, *Time-Harmonic Electromagnetic Fields*. Piscataway, NJ, USA: IEEE Press, 2001.

[28] K. Cools, F. P. Andriulli, D. D. Zutter, and E. Michielssen, "Accurate and conforming mixed discretization of the MFIE," *IEEE Antennas Wireless Propag. Lett.*, vol. 10, pp. 528–531, 2011.

[29] F. P. Andriulli et al., "A multiplicative Calderon preconditioner for the electric field integral equation," *IEEE Trans. Antennas Propag.*, vol. 56, no. 8, pp. 2398–2412, Aug. 2008.

[30] A. Buffa and S. H. Christiansen, "A dual finite element complex on the barycentric refinement," *Math. Comput.*, vol. 76, no. 260, pp. 1743–1769, Oct. 2007.

[31] T. F. Eibert, "Iterative-solver convergence for loop-star and loop-tree decompositions in method-of-moments solutions of the electric-field integral equation," *IEEE Antennas Propag. Mag.*, vol. 46, no. 3, pp. 80–85, Jun. 2004.

[32] F. P. Andriulli, K. Cools, I. Bogaert, and E. Michielssen, "On a well-conditioned electric field integral operator for multiply connected geometries," *IEEE Trans. Antennas Propag.*, vol. 61, no. 4, pp. 2077–2087, Apr. 2013.

[33] A. Merlini, Y. Beghein, K. Cools, E. Michielssen, and F. P. Andriulli, "Magnetic and combined field integral equations based on the quasi-Helmholtz projectors," *IEEE Trans. Antennas Propag.*, vol. 68, no. 5, pp. 3834–3846, May 2020.

[34] B. Hofmann, T. F. Eibert, F. P. Andriulli, and S. B. Adrian, "A low-frequency stable, excitation agnostic discretization of the right-hand side for the electric field integral equation on multiply-connected geometries," *IEEE Trans. Antennas Propag.*, early access, Jan. 11, 2023, doi: 10.1109/TAP.2023.3234704.

[35] R. Grech et al., "Review on solving the inverse problem in EEG source analysis," *J. Neuroeng. Rehabil.*, vol. 5, no. 1, p. 25, Dec. 2008. [Online]. Available: http://jneuroengrehab.biomedcentral.com/articles/10.1186/1743-0003-5-25

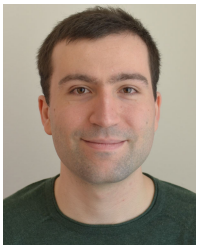

Paolo Ricci (Graduate Student Member, IEEE) received the B.Sc. and M.Sc. degrees in computer engineering from the Politecnico di Torino, Turin, Italy, in 2018 and 2020, respectively. He is currently pursuing the Ph.D. degree in the framework of a Marie Curie EID in collaboration with the Politecnico di Torino and Thales DMS France SAS, Élancourt, France.

In 2021, he joined the Politecnico di Torino as a Research Associate. His current research interests include computational electromagnetics with a focus on integral equation formulations, fast solvers, machine learning, and applications for antenna simulations and brain imaging.

Mr. Ricci has authored a paper that received an honorable mention in International Union of Radio Science (URSI)/IEEE–APS 2022.

Ermanno Citraro (Graduate Student Member, IEEE) received the B.Sc. and M.Sc. degrees in electrical engineering from the Politecnico di Torino, Turin, Italy, in 2017 and 2019, respectively, where he is currently pursuing the Ph.D. degree.

After a two years' working experience in the semiconductor industry, he joined the Politecnico di Torino as a Research Associate in 2021. His current research interests include computational electromagnetics, fast solvers, and brain imaging.

Mr. Citraro has authored a paper that received an honorable mention in International Union of Radio Science (URSI)/IEEE–APS 2022.

Adrien Merlini (Senior Member, IEEE) received the M.Sc.Eng. degree from the École Nationale Supérieure des Télécommunications de Bretagne (Télécom Bretagne), Brest, France, in 2015, and the Ph.D. degree from the École Nationale Supérieure Mines-Télécom Atlantique (IMT Atlantique), Brest, in 2019.

From 2018 to 2019, he was a Visiting Ph.D. Student with the Politecnico di Torino, Turin, Italy, where he then joined as a Research Associate. Since 2019, he has been an Associate Professor with the Microwave Department, IMT Atlantique. His research interests include preconditioning and acceleration of integral equation solvers for electromagnetic simulations and their application in brain imaging.

Dr. Merlini is a member of IEEE-Eta Kappa Nu (HKN), the IEEE Antennas and Propagation Society, International Union of Radio Science (URSI) France, and the Lab-STICC laboratory. He has received two Young Scientist Awards at the URSI General Assembly and Scientific Symposium (GASS) 2020 and the International Symposium on Electromagnetic Theory (EMTS) 2023 meetings. In addition, he has authored a paper that won third place at EMTS 2023 and coauthored a paper that received the 2022 International Conference on Electromagnetics in Advanced Applications (ICEAA)-IEEE Antennas and Propagation in Wireless Communications (APWC) Best Paper Award, five that received honorable mentions (URSI/IEEE–APS 2021, 2022, and 2023), and three Best Paper Finalists (URSI GASS 2020 and URSI/IEEE–APS 2021 and 2022). He has been serving as an Associate Editor for *IEEE Antennas and Propagation Magazine*.

Francesco P. Andriulli (Fellow, IEEE) received the Laurea degree in electrical engineering from the Politecnico di Torino, Turin, Italy, in 2004, the M.Sc. degree in electrical engineering and computer science from the University of Illinois at Chicago, Chicago, IL, USA, in 2004, and the Ph.D. degree in electrical engineering from the University of Michigan at Ann Arbor, Ann Arbor, MI, USA, in 2008.

From 2008 to 2010, he was a Research Associate with the Politecnico di Torino, where he has been a Full Professor since 2017. From 2010 to 2017, he was an Associate Professor (from 2010 to 2014) and then a Full Professor with the École Nationale Supérieure Mines-Télécom Atlantique (IMT Atlantique, previously ENST Bretagne), Brest, France. His research interests are in computational electromagnetics with a focus on frequency- and time-domain integral equation solvers, well-conditioned formulations, fast solvers, low-frequency electromagnetic analyses, and modeling techniques for antennas, wireless components, microwave circuits, and biomedical applications with a special focus on brain imaging.

Prof. Andriulli is a member of Eta Kappa Nu, Tau Beta Pi, Phi Kappa Phi, and the International Union of Radio Science (URSI). He has received several best paper awards at conferences and symposia (URSI National Assembly (NA) 2007, IEEE AP-S 2008, and International Conference on Electromagnetics in Advanced Applications (ICEAA) IEEE-Antennas and Propagation in Wireless Communications (APWC) 2015) also in co-authorship with his students and collaborators (ICEAA IEEE-APWC 2021, International Symposium on Electromagnetic Theory (EMTS) 2016, URSI-Deutschland (DE) Meeting 2014, and ICEAA 2009) with whom he also received a second prize conference paper (URSI General Assembly and Scientific Symposium (GASS) 2014), a third prize conference paper (IEEE–APS 2018), seven honorable mention conference papers (ICEAA 2011, URSI/IEEE–APS 2013, four in URSI/IEEE–APS 2022, and URSI/IEEE–APS 2023), and other three finalist conference papers (URSI/IEEE-APS 2012, URSI/IEEE-APS 2007, URSI/IEEE-APS 2006, and URSI/IEEE–APS 2022). He was a recipient of the 2014 IEEE AP-S Donald G. Dudley Jr. Undergraduate Teaching Award, the triennium 2014–2016 URSI Issac Koga Gold Medal, and the 2015 L. B. Felsen Award for excellence in electrodynamics. He has served as an Associate Editor for the IEEE TRANSACTIONS ON ANTENNAS AND PROPAGATION, IEEE ANTENNAS AND WIRELESS PROPAGATION LETTERS, IEEE ACCESS, and *IET Microwaves, Antennas and Propagation* (IET-MAP). He serves as a Track Editor for the IEEE TRANSACTIONS ON ANTENNAS AND PROPAGATION and an Associate Editor for *URSI Radio Science Letters*. He is the Editor-in-Chief of *IEEE Antennas and Propagation Magazine*. He is the PI of the ERC Consolidator Grant: 321—From Cubic^3 To^2 Linear^1 Complexity in Computational Electromagnetics.

Open Access funding provided by 'Politecnico di Torino' within the CRUI CARE Agreement